

Fast quantum gates based on Landau-Zener-Stückelberg-Majorana transitions

Joan J. Cáceres,^{1,*} Daniel Domínguez ,¹ and María José Sánchez ^{1,2}

¹*Centro Atómico Bariloche and Instituto Balseiro (Universidad Nacional de Cuyo), 8400 San Carlos de Bariloche, Río Negro, Argentina*

²*Instituto de Nanociencia y Nanotecnología, CONICET-CNEA, 8400 San Carlos de Bariloche, Río Negro, Argentina*



(Received 9 September 2023; accepted 9 November 2023; published 29 November 2023)

Fast quantum gates are of paramount importance for enabling efficient and error-resilient quantum computations. In the present work we analyze Landau-Zener-Stückelberg-Majorana (LZSM) strong driving protocols, tailored to implement fast gates with particular emphasis on small-gap qubits. We derive analytical equations to determine the specific set of driving parameters for the implementation of single-qubit and two-qubit gates employing single-period sinusoidal pulses. Our approach circumvents the need to scan experimentally a wide range of parameters and instead it allows to concentrate on fine-tuning the device near the analytically predicted values. We analyze the dependence of relaxation and decoherence on the amplitude and frequency of the pulses, obtaining the optimal regime of driving parameters to mitigate the effects of the environment. Our study focus on the single-qubit $X_{\frac{\pi}{2}}$, $Y_{\frac{\pi}{2}}$ and identity gates. Also, we propose the $\sqrt{\text{bSWAP}}$ as the simplest two-qubit gate attainable through a robust LZSM driving protocol.

DOI: [10.1103/PhysRevA.108.052619](https://doi.org/10.1103/PhysRevA.108.052619)

I. INTRODUCTION

One of the key ingredients in quantum computing is the ability to implement fast gates, which are the essential building blocks to perform quantum algorithms. In recent years, significant progress has been made in the design of quantum gates using superconducting qubits, which have become one of the most promising platforms due to their scalability, long coherence times, and potential for fast high-fidelity operations [1–3]. The transmon qubit [4] and the capacitively shunted flux qubit [5] establish the basis for modern design of artificial atoms based on superconducting circuits. A more recent addition, the fluxonium [6–11], has a low transition frequency and a large anharmonicity, making it a promising candidate for quantum simulations and high-fidelity gate operations.

A variety of techniques for implementing fast quantum gates, including dynamical decoupling, composite pulses, and optimal control, have been implemented so far [12–20]. These techniques have led to significant improvements in gate fidelity. However, most of them rely on a resonant Rabi driving with frequency $\omega \approx \Delta = E_1 - E_0$ (the qubit energy gap) and small amplitude, $A \ll \Delta$, whose duration is adapted to perform the target operation (throughout this article we take $\hbar = 1$). As the gate time t_g is inversely proportional to the generalized Rabi frequency, i.e., $t_g \propto \frac{1}{\Omega_R} \propto \frac{1}{A}$ [21], these schemes usually have limited gate speed involving time scales that are in conflict with those imposed by decoherence processes.

One approach to mitigate decoherence is to reduce the qubit coupling to the environment by using a low-frequency or small-gap qubit as the heavy fluxonium. However, again in these cases, methods based on the Rabi resonant control

would be unfeasible as Δ is small and in the rotating wave approximation (RWA), as $A \ll \Delta$ results in $t_g \gg t_\Delta = \frac{2\pi}{\Delta}$.

To circumvent the mentioned limitations, alternatives beyond the resonant Rabi protocol have been recently proposed to experimentally implement fast gates with t_g much smaller than the decoherence time [22–25]. One of these schemes is based on driving a composite qubit, formed by two capacitively coupled transmon qubits which have a small gap between two energy levels [23]. The qubit is controlled by a Landau-Zener-Stückelberg-Majorana (LZSM) driving protocol, which consists of driving the qubit with a strong amplitude and/or an off-resonant harmonic signal [26–30]. LZSM protocols have been successfully implemented in interferometry of superconducting qubits [31,32] and temporal oscillations [33], and used in the quantum simulation of universal conductance fluctuations and weak localization phenomena [34,35].

On the theoretical side, the study of the LZSM driving protocols requires the implementation of numerical methods, the most useful based on the Floquet formalism [28,36–38], as the RWA is valid in the weak driving and resonant cases, but breaks down in the strong driving regime where analytical and perturbative approaches fail. It is well known that the counterrotating terms lead to the shifts of resonances (Bloch-Siegert shift) and additional beat patterns in the time evolution [21,36] which are not captured in the RWA. In a quite recent paper [39], the Bloch-Siegert shift was calculated along the entire driving strength and frequency regime by a simple analytical method based on a self-consistent unitary transformation. The method uses a counterrotating hybridized rotating wave approximation (CHRW) [20,39,40] and enables to obtain an effective description of the qubit dynamics which reproduces the numerical results not only when the driving strength is moderately weak but also for large frequency and strong driving strengths, far beyond the perturbation theory.

*Present address: Quantronics group, Université Paris-Saclay, CEA, CNRS, SPEC, 91191 Gif-sur-Yvette Cedex, France.

In the present work, we conduct an analysis of LZSM strong driving protocols suitable for implementing quantum gates in small-gap qubits. By presenting precise analytical equations based on the CHRW approximation, we offer a method to determine the driving parameters (amplitude, frequency, initial and final idling times) required for both single-qubit gates and the $\sqrt{\text{bSWAP}}$ gate. The approach eliminates the need for extensive experimental parameter scanning, allowing to concentrate on fine-tuning the device based on the analytically predicted parameters. We suggest the $\sqrt{\text{bSWAP}}$ gate as an ideal two-qubit gate achievable through a straightforward single one-period sinusoidal pulse using the strong driving LZSM protocol.

The paper is organized as follows: In Sec. II we introduce the CHRW to analyze the effective dynamics of the driven qubit Hamiltonian in terms of the operator $U(T)$, for a single period T of a sinusoidal drive. As a figure of merit for the accuracy of the CHRW we compute the error of this approximation, defined in terms of the fidelity of the approximated evolution operator $U(T)$ with respect to the exact evolution operator (computed numerically). In Secs. III and IV we analyze the implementation of single-qubit $X_{\frac{\pi}{2}}$, $Y_{\frac{\pi}{2}}$ and two-qubit $\sqrt{\text{bSWAP}}$ gates, respectively, with special focus on the determination of the optimal driving parameters in order to engineer fast gates with strong nonresonant LZSM protocols based on single-period sinusoidal drives. The effect of relaxation and decoherence on the gate dynamics is analyzed in Sec. V. Finally, the summary and conclusions are presented in Sec. VI.

II. EFFECTIVE DYNAMICS FOR STRONGLY DRIVEN QUBITS

We start by considering the standard two-level Hamiltonian modeling a driven qubit,

$$H(t) = -\frac{\Delta}{2}\hat{\sigma}_z - \frac{\epsilon(t)}{2}\hat{\sigma}_x, \quad (1)$$

where $\hat{\sigma}_z$ and $\hat{\sigma}_x$ are the Pauli matrices and Δ is the qubit energy gap. The Hamiltonian is written in the basis spanned by the states $|0\rangle$ and $|1\rangle$, which correspond to the ground and excited states of the qubit, respectively. We consider a transverse driving protocol $\epsilon(t) = A \sin(\omega t)$, as used recently in small-gap qubits like superconducting composite qubits [23] and heavy fluxonium qubits [10,24].

For large-gap qubits, like the transmon, the driving strength A is typically small compared with the qubit gap Δ , in which case the qubit control is implemented in the Rabi-driving regime at resonant frequencies $\omega \approx \Delta$ that can be accurately described within the RWA. The recent development of highly coherent qubits with small gaps requires operation with nonresonant fast drives $\omega > \Delta$ and large driving amplitudes, using control protocols based on LZSM transitions [26,28–31]. In this case, and in contrast with the Rabi-driving protocol, there are no simple expressions to predict the driving parameters needed for the implementation of quantum gates. Instead, calibration protocols scanning the pulse amplitude A and frequency ω are usually performed in the experiments [10,23,24]. For instance, in Ref. [23], as a first step in the calibration protocol, the transition probability from the ground

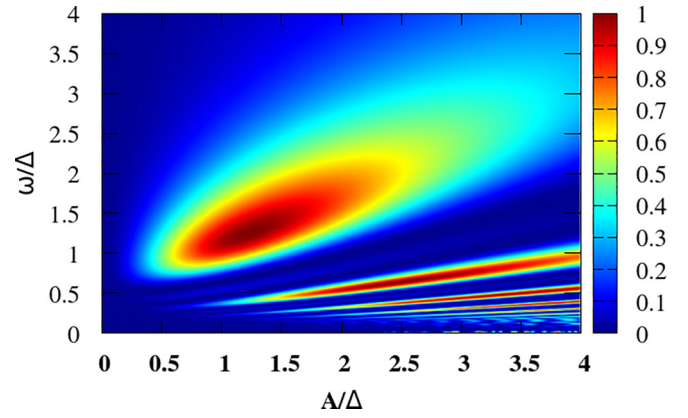


FIG. 1. Intensity plot of $P_{01} = |\langle 1|U_{\text{num}}(T)|0\rangle|^2$ as a function of the driving frequency ω and amplitude A , both normalized by the qubit gap Δ . P_{01} is computed numerically using a fourth-order Trotter-Suzuki algorithm. See text for details. The color bar indicates the probability P_{01} .

state to the excited state after a single period $T = 2\pi/\omega$ of the sinusoidal drive, $P_{01} \equiv P_{|0\rangle \rightarrow |1\rangle}(T)$, is measured as a function of A and ω . From this scanned transition probability, values of A and ω are chosen such that, for these values, P_{01} corresponds to the implementation of a given quantum gate. In a second calibration step, idling times before and after the driving pulse are finely tuned up in order to implement the desired quantum gate [23].

We have computed the time evolution with the $H(t)$ of Eq. (1) using a fourth-order Trotter-Suzuki algorithm [41], to compare with the calibration protocol of Ref. [23]. From the time evolution operator computed numerically, $U_{\text{num}}(t)$, we obtain $P_{01} = |\langle 1|U_{\text{num}}(T)|0\rangle|^2$ and plot it in Fig. 1 as a function of A and ω , scanning the same range of values as in the experiment. The computed probabilities align closely with the experimental results shown in Fig. S3 of Ref. [23].

An analytical accurate estimation of the amplitude and frequency of the driving pulse could greatly simplify the calibration procedure. The difficulty is that large driving strengths require to go beyond the RWA and to account for counterrotating effects. To obtain an effective description of the qubit dynamics one strategy is to use the CHRW approximation [20,39,40], applied to this case. To this end, we start with the transformation $|\psi'(t)\rangle = U_x|\psi(t)\rangle$, $H' = U_x H U_x^\dagger + i(\partial_t U_x)U_x^\dagger$, with $U_x = e^{-i\frac{\phi}{2}\hat{\sigma}_x}$. This gives [39]

$$H' = -\frac{(\epsilon - \dot{\phi})}{2}\hat{\sigma}_x - \frac{\Delta}{2}(\cos\phi\hat{\sigma}_z - \sin\phi\hat{\sigma}_y). \quad (2)$$

We take $\dot{\phi} = \xi\epsilon$, with ξ a parameter to be determined later. Thus, $\phi(t) = -\xi\frac{A}{\omega}\cos(\omega t)$ and $\exp(i\phi) = \exp[-i\xi\frac{A}{\omega}\cos(\omega t)]$. Using the Jacobi-Anger expansion in terms of Bessel functions for

$$e^{ix\cos a} = \sum_{k=-\infty}^{k=+\infty} i^k J_k(x) e^{ika} = J_0(x) + \sum_{k=1}^{\infty} 2i^k J_k(x) \cos(ka),$$

we approximate in Eq. (2) (to lowest order in the Fourier expansion)

$$\begin{aligned}\cos \phi &\approx J_0\left(\xi \frac{A}{\omega}\right) \\ \sin \phi &\approx -2J_1\left(\xi \frac{A}{\omega}\right) \cos(\omega t),\end{aligned}\quad (3)$$

and therefore

$$H' = -\frac{\epsilon(1-\xi)}{2} \hat{\sigma}_x - \frac{\Delta}{2} \left[J_0\left(\xi \frac{A}{\omega}\right) \hat{\sigma}_z + 2J_1\left(\xi \frac{A}{\omega}\right) \cos(\omega t) \hat{\sigma}_y \right],$$

which can be rewritten as

$$H' = -\frac{\tilde{\Delta}}{2} \hat{\sigma}_z - \frac{1}{2} [A(1-\xi) \sin(\omega t) \hat{\sigma}_x + 2\Delta J_1(a) \cos(\omega t) \hat{\sigma}_y], \quad (4)$$

with $\tilde{\Delta} = \Delta J_0(a)$ and $a = \xi A/\omega$.

After expressing ξ in terms of the self-consistent equation

$$A(1-\xi) = 2\Delta J_1\left(\xi \frac{A}{\omega}\right) = \tilde{A}, \quad (5)$$

we can rewrite Eq. (4) as

$$\begin{aligned}H' &= -\frac{\tilde{\Delta}}{2} \hat{\sigma}_z - \frac{\tilde{A}}{2} [\sin(\omega t) \hat{\sigma}_x + \cos(\omega t) \hat{\sigma}_y] \\ &= -\frac{\tilde{\Delta}}{2} \hat{\sigma}_z - \frac{\tilde{A}}{2} [-ie^{i\omega t} \hat{\sigma}_+ + ie^{-i\omega t} \hat{\sigma}_-],\end{aligned}\quad (6)$$

which can be solved exactly. After transforming with the unitary operator $R = e^{-i\frac{\tilde{\Delta}}{2}\hat{\sigma}_z}$, we obtain

$$H'' = RH'R^\dagger + i\frac{dR}{dt}R^\dagger = -\frac{\tilde{\delta}}{2} \hat{\sigma}_z - \frac{\tilde{A}}{2} \hat{\sigma}_y, \quad (7)$$

with $\tilde{\delta} = \tilde{\Delta} - \omega$.

Equation (7) can be easily diagonalized with the transformation $W = e^{-i\frac{\theta}{2}\hat{\sigma}_x}$, with $\tan \theta = \tilde{A}/\tilde{\delta}$, obtaining

$$H_d = WH''W^\dagger = -\frac{\Omega_R}{2} \hat{\sigma}_z, \quad (8)$$

with

$$\Omega_R = \sqrt{\tilde{\delta}^2 + \tilde{A}^2} = \sqrt{[\Delta J_0\left(\xi \frac{A}{\omega}\right) - \omega]^2 + 4\Delta^2 J_1^2\left(\xi \frac{A}{\omega}\right)}$$

the generalized Rabi frequency.

Taking into account the previous transformations, the evolution operator associated with Eq. (1), in the CHRW approximation, results in

$$U(t) = U_x^\dagger(t) R^\dagger(t) W^\dagger e^{i\frac{\Omega_R t}{2} \hat{\sigma}_z} W R(0) U_x(0). \quad (9)$$

In our case, for the implementation of fast quantum gates, we are interested in the evolution after one period of the driving T , which is

$$\begin{aligned}U(T) &= -e^{i\frac{\theta-a}{2}\hat{\sigma}_x} e^{i\frac{\pi\Omega_R}{\omega}\hat{\sigma}_z} e^{-i\frac{\theta-a}{2}\hat{\sigma}_x} \\ &= -\begin{pmatrix} \cos \alpha + i \sin \alpha \cos \tilde{\theta} & \sin \alpha \sin \tilde{\theta} \\ -\sin \alpha \sin \tilde{\theta} & \cos \alpha - i \sin \alpha \cos \tilde{\theta} \end{pmatrix},\end{aligned}\quad (10)$$

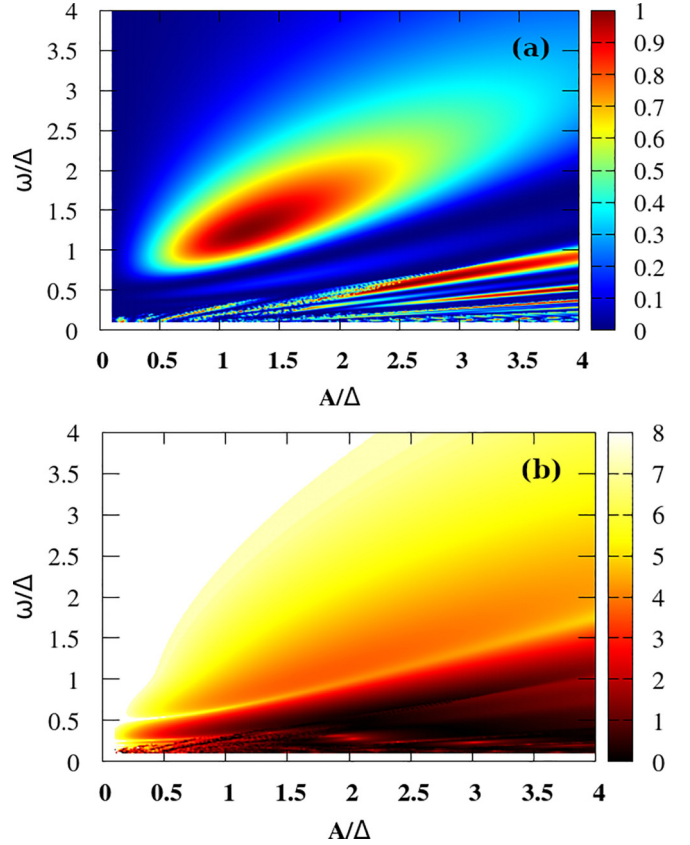


FIG. 2. (a) Transition probability P_{01} obtained from Eq. (11) as a function of driving frequency ω/Δ and amplitude A/Δ . The color bar indicates the probability P_{01} . (b) Intensity plot of the error \mathcal{E} of the CHRW approximation. The color bar indicates the logarithmic error $-\log_{10}|\mathcal{E}|$. Regions in white correspond to $\mathcal{E} < 10^{-8}$.

with $\alpha = \frac{\pi\Omega_R}{\omega}$ and $\tilde{\theta} = \theta - a = \theta - \xi \frac{A}{\omega}$. The transition probability between the qubit states, $|0\rangle \rightarrow |1\rangle$, can then be obtained in this approximation as

$$\begin{aligned}P_{01} &= |\langle 1|U(T)|0\rangle|^2 = \sin^2 \tilde{\theta} \sin^2 \alpha \\ &= \frac{[\tilde{A} \cos\left(\xi \frac{A}{\omega}\right) - \tilde{\delta} \sin\left(\xi \frac{A}{\omega}\right)]^2}{\Omega_R^2} \sin^2 \frac{\pi\Omega_R}{\omega}.\end{aligned}\quad (11)$$

In Fig. 2(a) we plot the transition probability computed from the analytical expression Eq. (11) as a function of the amplitude of the driving A/Δ and the frequency ω/Δ (both normalized in terms of the qubit gap). The agreement with the numerical result of Fig. 1 is remarkable, despite some noticeable differences in the range of small ω/A , due to numerical instabilities in the solution of Eq. (5) originated in the highly oscillatory behavior of the Bessel function $J_1(x)$ for large values of its argument x .

In order to check the accuracy of the CHRW approximation we compare the approximated $U(T)$ of Eq. (10) with the numerically exact $U_{\text{num}}(T)$. We quantify the error of the approximation as

$$\mathcal{E} = 1 - \mathcal{F} = 1 - \frac{\text{Tr}(U^\dagger U) + |\text{Tr}(U_{\text{ig}}^\dagger U)|^2}{d(d+1)}, \quad (12)$$

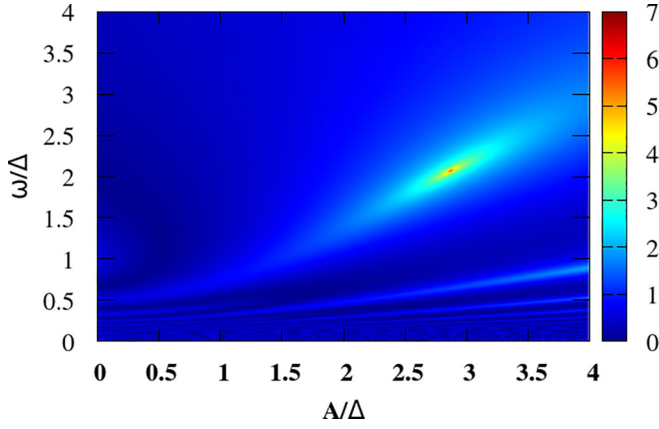


FIG. 3. Location of the parameters for implementation of the $Y_{\pi/2}$ gate. Intensity plot of the error function \mathcal{E} that compares the numerically exact evolution operator U_{num} with $Y_{\pi/2}$. The color bar corresponds to $-\log_{10} |\mathcal{E}|$. The point where $\mathcal{E} < 10^{-7}$ (practically zero within numerical precision) gives the operational parameters of the gate, frequency ω_Y and amplitude A_Y , which are in agreement with the analytical estimates of Eq. (14), $\omega_Y \approx 2.07\Delta$ and $A_Y \approx 2.87\Delta$.

where \mathcal{F} is the standard expression for the fidelity of an evolution operator U with respect to a target unitary operator U_{tg} [42]. In the present case is $U_{\text{tg}} = U_{\text{num}}(T)$, with $d = 2$ the dimension of the space, and $\text{Tr}(U^\dagger U) = d$, as $U(T)$ is exactly unitary. In Fig. 2(b) we plot the error \mathcal{E} . As expected [40], the CHRW approximation is very accurate in the range $\omega \gtrsim A/2$ and $\omega \gtrsim \Delta$ (with $\mathcal{E} \ll 10^{-3}$), which is also the range of interest for the experiment of Ref. [23]. Other methods of approximation such as the Magnus expansion (used in Ref. [10]) and the RWA in a double rotating frame (used in Refs. [43,44]) are less accurate (see Appendix B for a comparison of the different approximations).

In the following sections we shall analyze different implementations of single- and two-qubit gates following this driving protocol.

III. IMPLEMENTATION OF SINGLE-QUBIT GATES

Here, we analyze the conditions to implement fast single-qubit gates with a strong driving protocol based on nonresonant sinusoidal pulses [see Eq. (1)].

First, we note that $Z_\alpha = \exp(-i\alpha\hat{\sigma}_z/2)$ gates, can be realized by “idling” operations in the time evolution with the qubit set at $\epsilon = 0$ for a time $t = \alpha/\Delta$, as implemented in Ref. [23]. In addition to the continuous varying Z_α gate a complete set of single-qubit gates can be realized, implementing, for instance, $X_{\pm\pi/2} = \exp(\mp i\pi\hat{\sigma}_x/4)$ and $Y_{\pm\pi/2} = \exp(\mp i\pi\hat{\sigma}_y/4)$ gates.

In the case of the $Y_{\pi/2}$ gate, we can write it in matrix form as

$$Y_{\pi/2} = \frac{\sqrt{2}}{2} \begin{pmatrix} 1 & -1 \\ 1 & 1 \end{pmatrix}. \quad (13)$$

A direct comparison of Eq. (13) with the CHRW expression for the operator $U(T)$, Eq. (10), gives the following condition

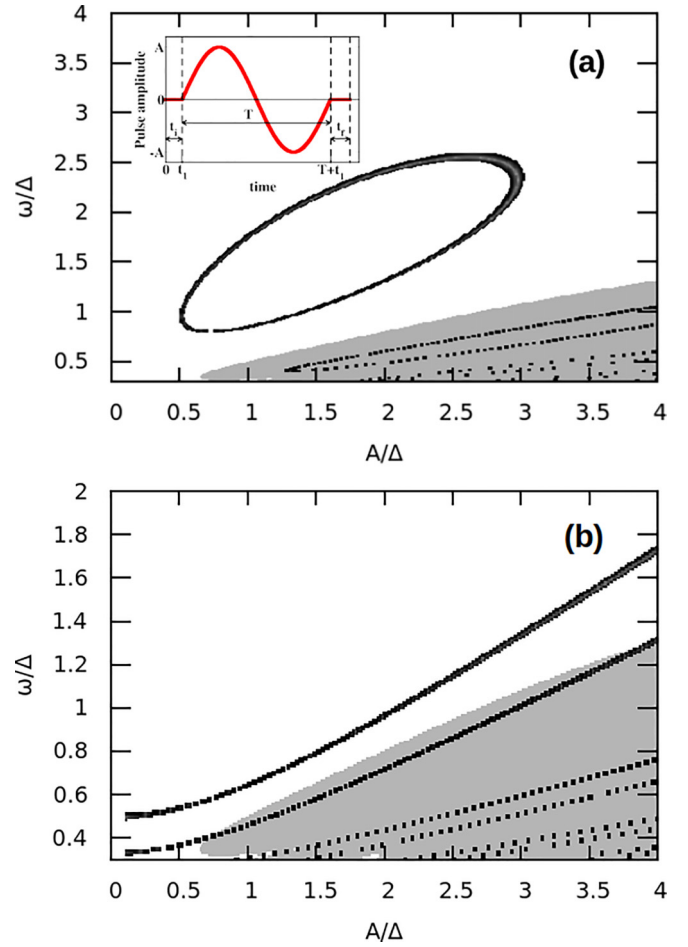


FIG. 4. (a) Plot of the parameter sets ω and A for the implementation of $X_{\pi/2}$ and $Y_{\pi/2}$ gates. The plotted points satisfy the analytical expressions of Eqs. (17) and (22) with a 10^{-3} accuracy (except for the low-frequency points, which correspond to the evaluation of the condition $P_{01} = 1/2$ with the same accuracy as the numerically exact evolution, since the CHRW approximation does not apply in this case). Inset: Schematic representation of the pulsing protocol with an idle time t_i added before the sinusoidal drive and a second idle time t_f afterwards. (b) Values of ω and A to implement the identity operation determined from Eq. (23), obtained with the same accuracy. In the regions shaded in gray the CHRW approximation has an error of 0.01, as analyzed in Fig. 2(b).

to implement the $Y_{\pi/2}$ gate with the largest ω :

$$\omega = \frac{4}{3}\Omega_R, \quad \theta - \xi \frac{A}{\omega} = \frac{\pi}{2}. \quad (14)$$

Numerical solution of these equations together with Eq. (5) give $\omega_Y \approx 2.07\Delta$ and $A_Y \approx 2.87\Delta$. The general conditions for the $Y_{\pi/2}$ gate are $\omega = \Omega_R/(2k + 3/4)$, $\tilde{\theta} = (2l + 1/2)\pi$ and $\omega = \Omega_R/(2k + 5/4)$, $\tilde{\theta} = (2l + 3/2)\pi$ for k, l integers. Solutions with $k \neq 0, l \neq 0$ give low ω and large A , beyond the parameter range for the CHRW approximation.

It is clear that the analytical estimate of the operational parameters for the gate implementation avoids the experimental cost of scanning parameters in a wide range. In the experiment, as described in the previous section, the fast gate is implemented applying the sinusoidal pulse for a single period

$T = 2\pi/\omega$, and the corresponding values of A and ω are determined by performing different measurements scanning the amplitude and frequency. In a similar way, we can compute numerically the exact evolution operator $U_{\text{num}}(T)$ varying the parameters ω and A , for instance, in the range $[0, 4\Delta]$. To obtain the numerically exact conditions for the $Y_{\frac{\pi}{2}}$ gate, we show in Fig. 3 the error function \mathcal{E} from Eq. (12) with $U = U_{\text{num}}(T)$ compared with the target $U_{\text{tg}} = Y_{\frac{\pi}{2}}$. The point of minimum \mathcal{E} [which is near the numerical precision for our calculation of $U_{\text{num}}(T)$, $\mathcal{E} \approx 10^{-7}$] corresponds to the operational point in A, ω for implementing the gate $Y_{\frac{\pi}{2}}$. This point agrees very accurately with the values (A_Y, ω_Y) computed previously from Eq. (14).

In the case of the $X_{\frac{\pi}{2}}$ gate, its matrix representation is

$$X_{\frac{\pi}{2}} = \frac{\sqrt{2}}{2} \begin{pmatrix} 1 & -i \\ -i & 1 \end{pmatrix}. \quad (15)$$

A comparison with the approximate $U(T)$ given in Eq. (10) shows that $X_{\frac{\pi}{2}}$ cannot be realized directly, since $\sin \alpha \sin \tilde{\theta} \neq i$. However, one can add after the sinusoidal pulse an idle (Z gate) evolution [23,45] during a time $t_f = \frac{\pi}{\Delta}$, such that

$$U(t_i + T + t_f) = \begin{pmatrix} -e^{i\tau_+} (\cos \alpha + i \sin \alpha \cos \tilde{\theta}) & -e^{i\tau_-} \sin \alpha \sin \tilde{\theta} \\ e^{-i\tau_-} \sin \alpha \sin \tilde{\theta} & -e^{-i\tau_+} (\cos \alpha - i \sin \alpha \cos \tilde{\theta}) \end{pmatrix}.$$

For both gates, $X_{\frac{\pi}{2}}$ and $Y_{\frac{\pi}{2}}$, the transition probability after one period is $P_{01} = |1|U|0\rangle|^2 = 1/2$, which corresponds to the implicit condition for ω and A given from the equation

$$\sin^2 \tilde{\theta} \sin^2 \alpha = \frac{1}{2}. \quad (17)$$

Thus, after imposing this condition in $U(t_i + T + t_f)$ one gets

$$U(t_i + T + t_f) = \frac{\sqrt{2}}{2} \begin{pmatrix} -e^{i(\tau_++\nu)} & -e^{i\tau_-} \\ e^{-i\tau_-} & -e^{-i(\tau_++\nu)} \end{pmatrix}, \quad (18)$$

where

$$\tan \nu = \tan \alpha \cos \tilde{\theta}. \quad (19)$$

Then, the $X_{\frac{\pi}{2}}$ gate can be obtained for

$$\begin{aligned} \tau_- &= (2n + 1/2)\pi \\ \tau_+ &= (2k + 1)\pi - \nu \end{aligned} \quad (20)$$

being k and n integers, while the $Y_{\frac{\pi}{2}}$ gate can be implemented for

$$\begin{aligned} \tau_- &= 2n\pi \\ \tau_+ &= (2k + 1)\pi - \nu, \end{aligned} \quad (21)$$

after straightforward comparisons with Eqs. (15) and (13), respectively.

To summarize, in order to determine the driving parameters ω, A, t_i, t_f for the gate implementation, one can proceed as follows. For a given driving frequency ω one obtains the possible amplitudes A after solving Eq. (17). Notice that since the relevant solutions of Eq. (17) are for $\omega > A$, it is very accurate to use for the ξ parameter the expression

$$\xi \approx \frac{\omega}{\omega + \Delta} \quad (22)$$

$e^{i\frac{\Delta}{\omega} \hat{\sigma}_z t_f} = i\hat{\sigma}_z$. Then, after the complete evolution given by $U(T + t_f) = i\hat{\sigma}_z U(T)$, the main conditions to implement a $X_{\frac{\pi}{2}}$ gate result in

$$\omega = 2\Omega_R, \quad \theta - \xi \frac{A}{\omega} = \frac{3\pi}{4}. \quad (16)$$

The numerical solution of these equations together with Eq. (5) gives $\omega_X \approx 0.81\Delta$ and $A_X \approx 0.68\Delta$. The general conditions for the $X_{\frac{\pi}{2}}$ gate are $\omega = \Omega_R/(2k + 1/2)$, $\tilde{\theta} = (2l + 3/4)\pi$ and $\omega = \Omega_R/(2k + 3/2)$, $\tilde{\theta} = (2l + 5/4)\pi$ for k, l integers.

The problem with the above conditions, Eqs. (14) and (16), is that each one requires very specific (and *different*) frequencies (ω_Y and ω_X) and gate times ($T_Y = 2\pi/\omega_Y$ and $T_X = 2\pi/\omega_X$) to implement them.

A more general procedure [23,45], which expands the possibilities in parameter space, is to add an idle time t_i before the sinusoidal drive and a second idle time t_f afterwards, see inset in Fig. 4(a). Calling $\tau_+ = (t_i + t_f)\Delta/2$ and $\tau_- = (t_f - t_i)\Delta/2$, the evolution operator in the CHRW approximation results in

from a first-order approximation of Eq. (5). The resulting points in A, ω space are shown in Fig. 4(a), where all the possible values for implementation of $X_{\frac{\pi}{2}}$ and $Y_{\frac{\pi}{2}}$ gates are plotted. Notice that the inclusion of idle times, implemented as rotations around the z axis, can steer any state represented by a point along the equator of the Bloch sphere to a rotated state represented by another point along the equator, leading to a ring of possible points in parameter space, in contrast to the case without the inclusion of idle times.

The points in Fig. 4(a) were obtained evaluating the above equations with an accuracy of 10^{-3} . In particular, we see in the plot that for large A and ω the conditions for the gate can be satisfied in a wider range of points for the same accuracy. We find in Fig. 4(a) that the relevant conditions for the $X_{\frac{\pi}{2}}$ and $Y_{\frac{\pi}{2}}$ fall within $\Delta \lesssim \omega \lesssim 3\Delta$ and $\Delta/2 \lesssim A \lesssim 3\Delta$.

Once the chosen driving parameters A, ω are determined from Eq. (17), the values of the idling times t_i and t_f needed to implement a $X_{\frac{\pi}{2}}$ or a $Y_{\frac{\pi}{2}}$ gate can be obtained from Eqs. (20) or (21), respectively.

It has been argued in Ref. [10] that, since different physical qubits could have different Δ parameters, it is useful to have *variable-time* single-qubit identity operations, to be able to perform operations in one qubit, avoiding having a second qubit acquire a dynamical phase at the same time. Comparing the CHRW expression of $U(T)$ given in Eq. (10) with the identity matrix, we obtain that the identity operation can be implemented for the A, ω that satisfy the simple condition

$$\omega = \Omega_R/(2k + 1). \quad (23)$$

The resulting values of A, ω are shown in Fig. 4(b), where we observe that in this case it is possible to use arbitrary large values of ω (and large A). On the other hand, for the $X_{\frac{\pi}{2}}$ and

$Y_{\frac{\pi}{2}}$ gates one can see in Fig. 4(a) that there is an upper limit in the frequency range for their implementation.

IV. TWO-QUBIT GATE: THE $\sqrt{\text{bSWAP}}$ GATE

Any universal quantum instruction set requires the implementation of at least one entangling two-qubit gate [1,3,46]. Here, we consider the parametrically driven two-qubit Hamiltonian:

$$H_{2q}(t) = -\frac{\Delta_1}{2}\hat{\sigma}_z \otimes I - \frac{\Delta_2}{2}I \otimes \hat{\sigma}_z - \frac{\epsilon(t)}{2}\hat{\sigma}_x \otimes \hat{\sigma}_x, \quad (24)$$

with driving in the coupling parameter $\epsilon(t) = A \sin(\omega t)$. Its matrix representation, using the basis $\{|00\rangle, |01\rangle, |10\rangle, |11\rangle\}$, is

$$H_{2q}(t) = -\frac{1}{2} \begin{pmatrix} \Delta_1 + \Delta_2 & 0 & 0 & \epsilon(t) \\ 0 & \Delta_1 - \Delta_2 & \epsilon(t) & 0 \\ 0 & \epsilon(t) & \Delta_2 - \Delta_1 & 0 \\ \epsilon(t) & 0 & 0 & -\Delta_1 - \Delta_2 \end{pmatrix}.$$

This two-qubit Hamiltonian with a $\hat{\sigma}_x \otimes \hat{\sigma}_x$ tunable coupling has been implemented, for example, in coupled fluxonium qubits [10,47,48].

In the following, we show that with a single-period sinusoidal drive, it is straightforward to get the $\sqrt{\text{bSWAP}}$ entangling gate [49–51]:

$$U_{\text{ent}} = \sqrt{\text{bSWAP}} = \begin{pmatrix} \frac{\sqrt{2}}{2} & 0 & 0 & -\frac{\sqrt{2}}{2} \\ 0 & 1 & 0 & 0 \\ 0 & 0 & 1 & 0 \\ \frac{\sqrt{2}}{2} & 0 & 0 & \frac{\sqrt{2}}{2} \end{pmatrix}, \quad (25)$$

which generates the entangled states $(|00\rangle \pm |11\rangle)/\sqrt{2}$ and leaves invariant the subspace spanned by $\{|01\rangle, |10\rangle\}$. It is easy to show that it is locally equivalent to the $\sqrt{\text{iSWAP}}$ gate [46,49].

The $\sqrt{\text{bSWAP}}$ gate can be exactly implemented in the ideal case when both qubits have equal gaps, $\Delta_1 = \Delta_2 = \Delta$. To demonstrate its realization, we calculate the error function \mathcal{E} of the exact evolution operator $U_{\text{num},2q}(T)$, computed numerically from $H_{2q}(t)$, compared with the target gate $U_{\text{tg}} = U_{\text{ent}}$, as a function of the parameters ω and A . In the plot of Fig. 5(a) we find a point A_{bS}, ω_{bS} with a minimum \mathcal{E} , near the numerical accuracy, which shows that it is possible to implement the $\sqrt{\text{bSWAP}}$ gate with this protocol. To illustrate the dynamical process that leads to the $\sqrt{\text{bSWAP}}$ gate, we show in Fig. 5(b) the time evolution of the population transfers during a driving period at ω_{bS}, A_{bS} . Furthermore, in Fig. 5(c) we see that in a nonideal case, when there is a small difference in the gaps of the qubits, $\Delta_2 = 1.05\Delta_1$, the $\sqrt{\text{bSWAP}}$ gate can be reproduced at a slightly shifted operational point and with error $\mathcal{E} \approx 10^{-6}$.

We can proceed as in the previous section in order to provide an analytical estimate of the parameters for the $\sqrt{\text{bSWAP}}$. To use the CHRW approximation of Sec. II it is convenient to transform $H_{2q}(t)$ to $\tilde{H}_{2q} = SH_{2q}S^\dagger$ with

$$S = \begin{pmatrix} 1 & 0 & 0 & 0 \\ 0 & 0 & 0 & 1 \\ 0 & 0 & 1 & 0 \\ 0 & 1 & 0 & 0 \end{pmatrix},$$

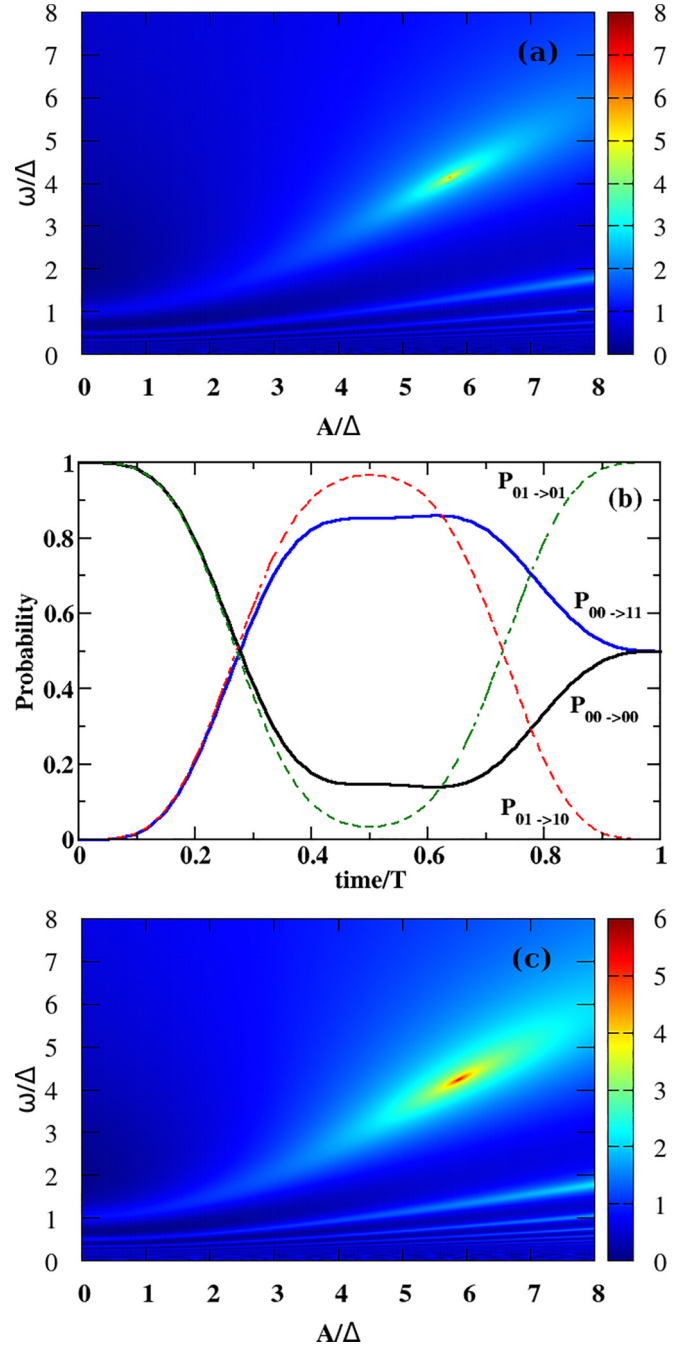


FIG. 5. (a) Plot, as a function of the parameters A and ω , of the error \mathcal{E} that compares $\sqrt{\text{bSWAP}}$ with the numerically exact $U_{\text{num},2q}$, computed from H_{2q} Eq. (24). The color bar scale corresponds to $-\log_{10} |\mathcal{E}|$. The point where $\mathcal{E} < 10^{-7}$ (practically zero within numerical precision) gives the operational parameters of the gate, frequency ω_{bS} and amplitude A_{bS} . It agrees with the analytical estimate of $\omega_{bS} \approx 4.14\Delta$, $A_{bS} \approx 5.74\Delta$. (b) Time evolution of the population transfers during a driving period for ω_{bS}, A_{bS} . Continuous lines correspond to the evolution of the populations of the $|00\rangle$ (black) and the $|11\rangle$ states (blue), after the initial state $|00\rangle$. Dashed lines correspond to the evolution of the populations of the $|01\rangle$ (green) and the $|10\rangle$ states (red), after the initial state $|01\rangle$. (c) Same as (a) but for two slightly different qubits with $\Delta_2 = 1.05\Delta_1$. See text for more details.

obtaining

$$\widetilde{H}_{2q}(t) = -\frac{1}{2} \begin{pmatrix} \Delta_1 + \Delta_2 & \epsilon(t) & 0 & 0 \\ \epsilon(t) & -\Delta_1 - \Delta_2 & 0 & 0 \\ 0 & 0 & \Delta_2 - \Delta_1 & \epsilon(t) \\ 0 & 0 & \epsilon(t) & \Delta_1 - \Delta_2 \end{pmatrix},$$

which separates into two independent blocks,

$$\begin{aligned} \widetilde{H}_{2q}(t) &= \left[-\frac{\Delta_+}{2} \hat{\sigma}_z - \frac{\epsilon(t)}{2} \hat{\sigma}_x \right] \otimes \begin{pmatrix} 1 & 0 \\ 0 & 0 \end{pmatrix} \\ &+ \left[-\frac{\Delta_-}{2} \hat{\sigma}_z - \frac{\epsilon(t)}{2} \hat{\sigma}_x \right] \otimes \begin{pmatrix} 0 & 0 \\ 0 & 1 \end{pmatrix}, \end{aligned} \quad (26)$$

with $\Delta_+ = \Delta_1 + \Delta_2$ and $\Delta_- = \Delta_2 - \Delta_1$. Thus, in this basis we can express the evolution operator \widetilde{U}_{2q} in terms of single-qubit operators as

$$\widetilde{U}_{2q}(t) = U_+(t) \otimes \begin{pmatrix} 1 & 0 \\ 0 & 0 \end{pmatrix} + U_-(t) \otimes \begin{pmatrix} 0 & 0 \\ 0 & 1 \end{pmatrix}, \quad (27)$$

where U_+ (U_-) is equal to the single-qubit evolution operator after replacing Δ with Δ_+ (Δ_-). It is now straightforward to obtain the evolution operator in the CHRW approximation, following the same steps as in the single-qubit case for U_+ and U_- . After one period T , and transforming back to the original basis, we obtain

$$U_{2q}(T) = - \begin{pmatrix} a_+ & 0 & 0 & b_+ \\ 0 & a_-^* & b_- & 0 \\ 0 & -b_- & a_- & 0 \\ -b_+ & 0 & 0 & a_+^* \end{pmatrix}, \quad (28)$$

with

$$\begin{aligned} a_+ &= \cos \alpha_+ + i \sin \alpha_+ \cos \tilde{\theta}_+ \\ b_+ &= \sin \alpha_+ \sin \tilde{\theta}_+ \\ a_- &= \cos \alpha_- + i \sin \alpha_- \cos \tilde{\theta}_- \\ b_- &= \sin \alpha_- \sin \tilde{\theta}_-, \end{aligned}$$

where $\alpha_{+(-)}$, $\tilde{\theta}_{+(-)}$ are obtained as in Sec. II after replacing $\Delta \rightarrow \Delta_+$ (Δ_-) in the generalized Rabi frequency $\Omega_R \rightarrow \Omega_{+R}$ (Ω_{-R}) and $(..)^*$ denotes the complex conjugate operation.

When $\Delta_1 = \Delta_2 = \Delta$, since $\Delta_- = 0$, we have

$$U_{2q}(T) = \begin{pmatrix} -a_+ & 0 & 0 & -b_+ \\ 0 & 1 & 0 & 0 \\ 0 & 0 & 1 & 0 \\ b_+ & 0 & 0 & -a_+^* \end{pmatrix}. \quad (29)$$

Therefore, to obtain the $\sqrt{\text{bSWAP}}$ gate, a comparison with Eq. (25) gives $b_+ = -a_+ = \frac{\sqrt{2}}{2}$ with $\Delta_+ = 2\Delta$, and the main conditions are

$$\omega = \frac{4}{3} \Omega_{+R}, \quad \theta_+ - \xi_+ \frac{A}{\omega} = \frac{\pi}{2}. \quad (30)$$

The numerical solution of these equations gives $\omega_{bS} = 4.14\Delta$, $A_{bS} = 5.74\Delta$, which coincide with the optimal point of Fig. 5(a). (Note that they are the same as for the $Y_{\frac{\pi}{2}}$ gate after the substitution $\Delta \rightarrow 2\Delta$, and so similarly the general conditions can be obtained.)

As in the single-qubit case, for the $\sqrt{\text{bSWAP}}$ gate we can extend the set of parameters to those A, ω which satisfy

$P_{00 \rightarrow 11} = 1/2$. It is straightforward to show that this set is obtained from the solution of

$$\begin{aligned} P_{00 \rightarrow 11} &= |\langle 11 | U_{2q}(T) | 00 \rangle|^2 \\ &= \sin^2 \tilde{\theta}_+ \sin^2 \alpha_+ = \frac{1}{2}. \end{aligned} \quad (31)$$

To implement the $\sqrt{\text{bSWAP}}$ gate for the parameters satisfying the above equation, one has to add an idle time t_i before the sinusoidal drive and a second idle time t_f afterwards. Calling $\tau_+ = (t_1 + t_2)\Delta$, $\tau_- = (t_2 - t_1)\Delta$, we have

$$U(t_i + T + t_f) = e^{i\frac{\tau_+}{2}(\hat{\sigma}_z \otimes I + I \otimes \hat{\sigma}_z)} U(T) e^{i\frac{\tau_-}{2}(\hat{\sigma}_z \otimes I + I \otimes \hat{\sigma}_z)} \quad (32)$$

$$= \begin{pmatrix} -e^{i\tau_+} a_+ & 0 & 0 & -e^{i\tau_-} b_+ \\ 0 & 1 & 0 & 0 \\ 0 & 0 & 1 & 0 \\ e^{-i\tau_-} b_+ & 0 & 0 & -e^{-i\tau_+} a_+^* \end{pmatrix}. \quad (33)$$

Defining $\rho e^{i\nu} = \cos \alpha_+ + i \sin \alpha_+ \cos \tilde{\theta}_+$, where $\tan \nu = \tan \alpha_+ \cos \tilde{\theta}_+$, we can write

$$\begin{pmatrix} -\rho e^{i(\tau_+ + \nu)} & 0 & 0 & \mp e^{i\tau_-} \sqrt{1 - \rho^2} \\ 0 & 1 & 0 & 0 \\ 0 & 0 & 1 & 0 \\ \pm e^{-i\tau_-} \sqrt{1 - \rho^2} & 0 & 0 & -\rho e^{-i(\tau_+ + \nu)} \end{pmatrix}. \quad (34)$$

For the case $P_{00 \rightarrow 11} = 1 - \rho^2 = 1/2$ this corresponds to

$$\begin{pmatrix} \frac{\sqrt{2}}{2} e^{i(\tau_+ + \nu)} & 0 & 0 & \mp \frac{\sqrt{2}}{2} e^{i\tau_-} \\ 0 & 1 & 0 & 0 \\ 0 & 0 & 1 & 0 \\ \pm \frac{\sqrt{2}}{2} e^{-i\tau_-} & 0 & 0 & \frac{\sqrt{2}}{2} e^{-i(\tau_+ + \nu)} \end{pmatrix}. \quad (35)$$

Then, the $\sqrt{\text{bSWAP}}$ gate can be obtained for $\tau_- = 2k\pi$ and $\tau_+ + \nu = (2n + 1)\pi$.

This gate is robust against a small difference in the parameters of the two qubits. For $\Delta_2 - \Delta_1 = \epsilon\Delta$, the invariance under gate operation of the subspace spanned by $\{|01\rangle, |10\rangle\}$ cannot be attained exactly. Then, the error in the gate operation can be estimated from evaluating the probability $P_{|10\rangle \rightarrow |01\rangle}$, which should be zero for a perfect gate. For $\epsilon \ll 1$ we estimate the error from Eq. (28) as $\mathcal{E}_\epsilon \propto P_{|10\rangle \rightarrow |01\rangle} = b_-^2 \approx \epsilon^2 \pi^2 \left(\frac{\Delta}{\omega}\right)^2 J_0^2\left(\frac{\Delta}{\omega}\right) \sin^2\left(\frac{\Delta}{\omega}\right)$. For the case (A_{bS}, ω_{bS}) and $\epsilon = 0.01$ the error is $\mathcal{E}_{0.01} \approx 2 \times 10^{-5}$ and it decreases as $\sim \omega^{-2}$ for increasing ω .

V. RELAXATION AND DECOHERENCE UNDER STRONG DRIVE

In the previous sections we have found more than one choice for the operational parameters ω, A to implement single-qubit and two-qubit gates with a LZSM protocol. In this section we analyze the environmental influences on the gate fidelity. It has been shown by Chow *et al.* [52] that the limits on gate fidelity are imposed by qubit decoherence, and that gate errors scale as $\Gamma_1 t_g$, with Γ_1 the relaxation rate and t_g the gate time length. For weak drives, the main dependence of transition rates is given by the bath temperature and the system-environment coupling strength. On the other hand, it

is known that for strong driving the transition rates also depend on the driving parameters [28,38,53–56]. Therefore, the dependence of relaxation and decoherence rates on ω , A has to be considered to optimize the fidelity in the implementation of qubit gates under these protocols (at fixed temperature and system-reservoir coupling strength). We will discuss here the single-qubit case, but the analysis can be extended straightforwardly for the case of two qubits considering that the dynamics of the Hamiltonian of Eq. (24) can be transformed to the dynamics of two independent qubits as shown in Eqs. (26) and (27).

The effect of the environment can be described by the global Hamiltonian $\mathcal{H}(t) = H_s(t) + H_b + H_{sb}$, where $H_s(t) = H_s(t + T)$ is the Hamiltonian of the driven qubits with time period $T = 2\pi/\omega$. The Hamiltonian H_b corresponds to a thermal bath and $H_{sb} = \hat{O} \otimes \hat{B}$ is the system-bath coupling term, with \hat{B} representing the quantum noise due to the bath and \hat{O} is the observable of the system coupled to the noise.

The natural basis to compute relaxation and decoherence rates in the case of strong time periodic drives is the Floquet basis [36], since in this basis the density matrix in the steady state becomes diagonal [38,53,54,57–62]. In the case of a two-level system, like the Hamiltonian of Eq. (1), the wave functions have the time dependence $|\Psi(t)\rangle = c_a e^{-i\epsilon_a t} |a(t)\rangle + c_b e^{-i\epsilon_b t} |b(t)\rangle$, where the Floquet states $|a(t)\rangle$, $|b(t)\rangle$ are periodic with time period T , and ϵ_a , ϵ_b are the associated quasienergies [36,54,57,63]. In the CHRW approximation, $|a(t)\rangle$ and $|b(t)\rangle$ can be obtained from the eigenstates of the static Hamiltonian H'' , Eq. (7), after performing on them a time-dependent transformation back to the representation of the original Hamiltonian Eq. (1). In the limit $A \rightarrow 0$ the Floquet states tend to the eigenstates of the undriven Hamiltonian: $|a(t)\rangle \rightarrow |0\rangle$, $|b(t)\rangle \rightarrow |1\rangle$, and similarly the Floquet gap $\Delta_F = |\epsilon_b - \epsilon_a|$ tends to the undriven gap, $\Delta_F \rightarrow \Delta = E_1 - E_0$.

From the Floquet-Markov quantum master equation (see Appendix A) the relaxation rate can be obtained as

$$\begin{aligned} \Gamma_1 &= \sum_{q=-\infty}^{+\infty} S(\epsilon_b - \epsilon_a + q\omega) \left| \frac{1}{T} \int_0^T \langle a(t) | \hat{O} | b(t) \rangle e^{iq\omega t} dt \right|^2 \\ &\approx S(\Delta_F) \left| \frac{1}{T} \int_0^T \langle a(t) | \hat{O} | b(t) \rangle dt \right|^2, \end{aligned} \quad (36)$$

where $S(\Omega)$ is the noise power spectrum. The second line of Eq. (36) approximates Γ_1 with the $q = 0$ term, which is the dominant contribution in the sum of the first line. It is also direct to show that in the undriven limit, $A \rightarrow 0$, we can recover the standard result $\Gamma_1 = S(\Delta) |\langle 0 | \hat{O} | 1 \rangle|^2$.

We consider here that the main source of quantum noise is through the same channel as the driving, and thus we take for the noise coupling operator $\hat{O} = \hat{\sigma}_x$. An approximate expression of Γ_1 can be obtained calculating the matrix elements $\langle a(t) | \hat{\sigma}_x | b(t) \rangle$ in the CHRW approximation (see Appendix A),

$$\Gamma_1 \approx S(\Delta_F) \cos^4 \frac{\theta}{2}, \quad (37)$$

where $\Delta_F = |\Omega_R - \omega|$ in this case. We have calculated the dependence of Γ_1 with the frequency ω and the amplitude A considering noise with power spectrum $S(\Omega) =$

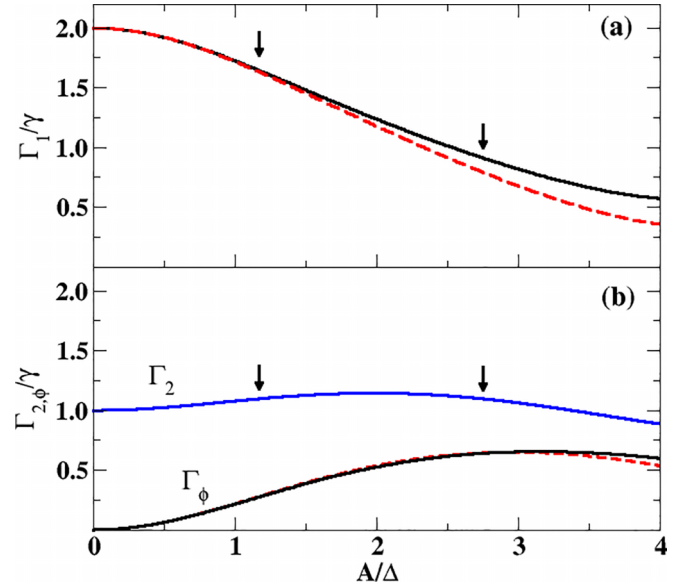


FIG. 6. (a) Plot of the relaxation rate Γ_1 as a function of A/Δ for $\omega = 1.92\Delta$. The black continuous line corresponds to the numerically exact value and the dashed line the CHRW approximation, Eq. (37). (b) Plot of the dephasing rate Γ_ϕ as a function of A/Δ for $\omega = 1.92\Delta$. The black continuous line corresponds to the numerically exact value and the dashed line to the CHRW approximation. Also, the decoherence rate Γ_2 is plotted (blue continuous line, numerically exact values only). In both (a) and (b), the arrows indicate the values of A where the $X_{\pi/2}$, $Y_{\pi/2}$ gates can be implemented, as obtained from Fig. 4(a); the rates Γ_1 , Γ_ϕ , Γ_2 are normalized by the noise strength parameter γ and correspond to a thermal bath at temperature $T_b = 0.1\Delta$.

$2\gamma\Omega \coth(\Omega/2T_b)$. We obtain the values of Γ_1 normalized by the noise strength parameter γ . In order to see more clearly the dependence with the driving parameters, we show the case for a low temperature $T_b = 0.1\Delta$. We find that the general behavior for $\omega > \Delta$ is that the relaxation rate decreases with increasing A , as seen in Fig. 6(a) for frequency $\omega = 1.96\Delta$ in the range of interest [64]. Higher temperatures ($T_b \gtrsim \Delta$) give a similar behavior but with a milder dependence with A . The arrows in Fig. 6(a) indicate the values of A for which the $X_{\pi/2}$, $Y_{\pi/2}$ gates could be implemented at this driving frequency, as obtained from Fig. 4(a). Considering that Γ_1 is smaller for larger A , the value indicated by the second arrow in the plot should be the preferred choice for a reduced effect of the environment in the qubit dynamics. We also plot in Fig. 6(a) the CHRW approximation of Eq. (37) and the numerically exact evaluation of Eq. (36) (after calculating the Floquet states and quasienergies and summing terms in q up to ± 32), showing that they are in good agreement.

To complete the analysis of the effect of the environment, we have to calculate the decoherence rate $\Gamma_2 = \Gamma_1/2 + \Gamma_\phi$. The dephasing rate Γ_ϕ can be obtained from the Floquet-Markov quantum master equation as

$$\Gamma_\phi = \sum_{q \geq 0} 2S(q\omega) \left| \frac{1}{T} \int_0^T dt \langle a(t) | \hat{O} | a(t) \rangle e^{iq\omega t} \right|^2. \quad (38)$$

In the case under consideration, with noise coupling operator $\hat{O} = \hat{\sigma}_x$, the $q = 0$ term is exactly zero. Moreover, in the undriven limit $A \rightarrow 0$ the dephasing rate completely vanishes, $\Gamma_\phi^{A \rightarrow 0} = 0$, corresponding to the fact that the qubit of Eq. (1) is in a “sweet spot” [23]. But, for finite driving, the $q \neq 0$ terms start to contribute to dephasing, with the dominant term being the $q = 1$ term, leading to the expression

$$\Gamma_\phi \approx 2S(\omega) \left| \frac{1}{T} \int_0^T dt \langle a(t) | \hat{\sigma}_x | a(t) \rangle e^{i\omega t} \right|^2. \quad (39)$$

In this case, the CHRW approximation gives

$$\Gamma_\phi \approx 2S(\omega) \left[\sin \theta (J_0 + J_2) + \sin^2 \frac{\theta}{2} (J_1 + J_3) \right]^2, \quad (40)$$

where we have denoted $J_l \equiv J_l(\xi A/\omega)$. We plot in Fig. 6(b) the dephasing rate Γ_ϕ as a function of A for $\omega = 1.96\Delta$. As stated, we find that $\Gamma_\phi = 0$ for $A = 0$, and then that Γ_ϕ increases for increasing A . Therefore, dephasing is increased by the driving, which is in the opposite direction as the effect of driving on the relaxation rate, analyzed in the previous paragraph. However, to determine the optimal parameters for the gate, one has to analyze the decoherence rate Γ_2 that combines dephasing and relaxation. As can be seen in Fig. 6(b), the decoherence rate changes mildly as a function of the driving strength A , being nearly the same for the two cases indicated by the arrows. Therefore, considering the previously discussed driving effect on relaxation, the larger A is still the better choice for the implementation of the gates. We also compare in Fig. 6(b) the approximated and the numerically exact Γ_ϕ , which are in good agreement.

When considering lower ω the behavior of Γ_1 and Γ_2 is more complex. In Figs. 7(a) and 7(b) we show intensity plots of Γ_1 and Γ_2 , respectively, as a function of A and ω , plotting the numerically exact values in the full range of ω (the approximated values discussed above are accurate only for $\omega > \Delta$). We also plot in Fig. 7 (with black dots) the values of A , ω corresponding to the conditions for the implementation of the $X_{\pi/2}$, $Y_{\pi/2}$ gates. The relaxation rate Γ_1 decreases for increasing A for any of the frequencies in the range of interest ($\omega \gtrsim \Delta$), thus large A would always be more convenient for gate implementations in order to minimize relaxation. In the plot of Fig. 7(a) this corresponds to the gate parameters that fall within the blue region (which indicates lowest values of Γ_1 in the color scale of the plot).

On the other hand, the decoherence rate Γ_2 is large in the regions near resonance $\omega \sim \Delta$ and for $A \lesssim 2\Delta$, within the red region in Fig. 7(b). This behavior is almost independent of temperature, i.e., higher temperatures ($T_b \gtrsim \Delta$) give similar plots except for a larger overall value of Γ_2 , because the relevant dependence is on the matrix element $|\frac{1}{T} \int_0^T dt \langle a(t) | \hat{\sigma}_x | a(t) \rangle e^{i\omega t}|^2$. Therefore, off-resonant large-frequency driving is always more convenient for the gates analyzed here, since for $\omega \gg \Delta$ the decoherence rate is low and nearly insensitive to variations in the driving amplitude A .

The combined analysis of the competing conditions for minimal relaxation and minimal decoherence leads to the conclusion that the best parameters for the implementation of

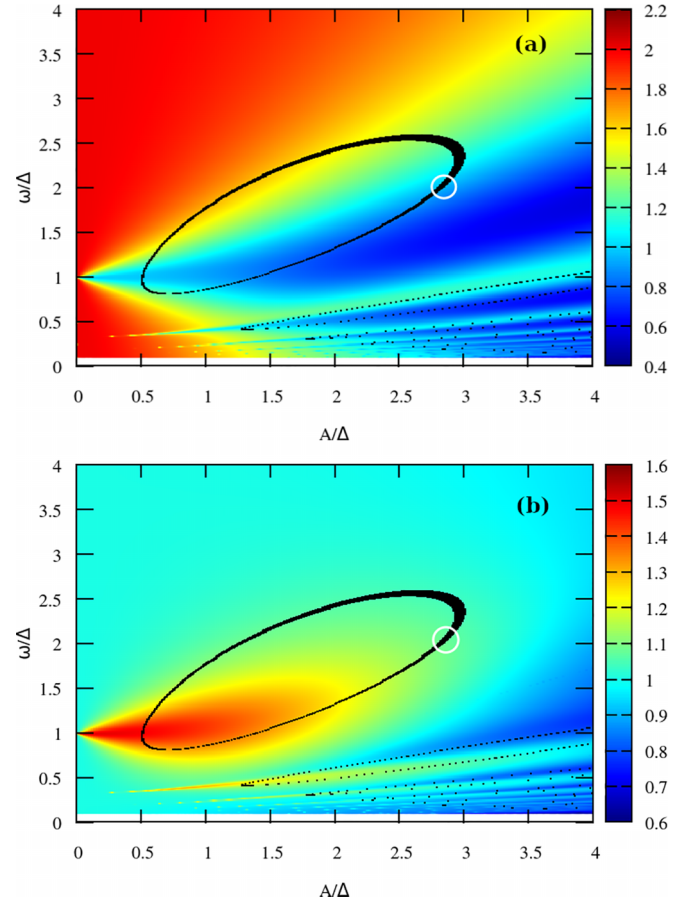


FIG. 7. Intensity plot of (a) the relaxation rate Γ_1 and (b) the decoherence rate Γ_2 , as a function of A/Δ and ω/Δ . The black dots indicate the parameter sets ω and A for the implementation of $X_{\pi/2}$ and $Y_{\pi/2}$ gates, as in Fig. 4(a). The white circle shows the optimal parameter region to minimize environmental effects. All rates correspond to a bath at temperature $T_b = 0.1\Delta$. The color bar scale corresponds to the rates Γ_1, Γ_2 normalized by the noise strength parameter γ .

the $X_{\pi/2}$, $Y_{\pi/2}$ gates are within the region in A , ω highlighted with a circle in Fig. 7.

VI. SUMMARY AND CONCLUSIONS

We have analyzed LZSM strong driving protocols for the implementation of quantum gates which are well suited for small gap qubits. We provide accurate analytical equations to obtain the driving parameters (amplitude, frequency, initial and final idling times) for single-qubit gates and for the $\sqrt{\text{bSWAP}}$ two-qubit gate. Our approach avoids the need to scan experimentally a wide range of parameters and instead it allows to focus on fine-tuning the device near the analytically predicted parameters.

We have found that the $X_{\pi/2}$ and $Y_{\pi/2}$ gates can be efficiently implemented with a single strong one-period sinusoidal drive, with parameters in the range $\Delta \lesssim \omega \lesssim 3\Delta$ and $\Delta/2 \lesssim A \lesssim 3\Delta$. We note that the $X_{\pi/2}$ and $Y_{\pi/2}$ gates could also be implemented using a half-period sinusoidal drive, which would allow for operation at even larger amplitudes and frequencies [it is easy in the CHRW calculation to obtain the $U(T/2)$ operator and the corresponding conditions for the gates]. However,

a one-period sinusoidal drive is preferred since it has zero time integral and thus the dc components associated with pulse transients cancel out [23].

The high amplitude and high frequency of the sinusoidal pulses make it necessary to take into account the dependence of relaxation and decoherence with the driving parameters. We have shown that relaxation decreases with increasing amplitude. Therefore, large A should be preferred. However, leakage to higher energy levels could induce gate errors for large drives. This effect depends on the specific multilevel structure of the quantum device. A rule-of-thumb argument is that the amplitude A should be smaller than $E_2 - E_1$, with E_2 the energy of the third level (and E_0, E_1 the qubit two-level energies), to avoid leakage effects. In the optimal region signaled in Fig. 7 we find $A \sim 3\Delta$ for minimal relaxation, then requiring $E_2 - E_1 \gg 3(E_1 - E_0)$. Most superconducting qubit devices fulfill this condition. Decoherence is much smaller in the off-resonant case, for frequencies $\omega > \Delta$. Considering that the gate time is given by the driving period, $t_g \sim T$, the gate error [52] due to relaxation can be estimated as proportional to $\Gamma_1 T = 2\pi\Gamma_1/\omega$, and similarly the error due to decoherence as proportional to $2\pi\Gamma_2/\omega$. Therefore, high frequencies, which imply faster gates, are always preferred to reduce the detrimental effects of the environment.

Here, we propose the $\sqrt{\text{bSWAP}}$ gate as the simplest two-qubit gate that can be implemented with a strong driving LZSM protocol. Previous implementations of the $\sqrt{\text{bSWAP}}$ gate used protocols based on two-photon transitions [49–51]. The protocol based on LZSM transitions proposed here only requires a single one-period sinusoidal pulse, and thus it can be easier to realize, and possibly faster, than the “two-photon” protocols. Therefore, we consider it to be worthwhile to implement in the future this two-qubit gate in small-gap superconducting qubits.

ACKNOWLEDGMENTS

We acknowledge support from CNEA, CONICET, AN-PCyT (PICT2019-0654), and UNCuyo (06/C026-T1).

APPENDIX A: FLOQUET STATES AND QUANTUM MASTER EQUATION

1. Floquet states

Consider the two-level Hamiltonian:

$$H(t) = -\frac{\Delta}{2}\hat{\sigma}_z - \frac{\epsilon(t)}{2}\hat{\sigma}_x, \quad (\text{A1})$$

with $\epsilon(t) = A \sin(\omega t)$.

According to the Floquet theorem for time-periodic Hamiltonians, the solutions of the Schrödinger equation are of the form $|\Psi_\alpha(t)\rangle = e^{i\epsilon_\alpha t/\hbar}|u_\alpha(t)\rangle$, where the Floquet states $|u_\alpha(t)\rangle$ satisfy $|u_\alpha(t)\rangle = |u_\alpha(t+T)\rangle$ and are eigenstates of $[H_s(t) - i\hbar\partial/\partial t]|u_\alpha(t)\rangle = \epsilon_\alpha|u_\alpha(t)\rangle$, with ϵ_α the associated quasienergy [36,54,57]. The evolution operator can be written in matrix form as

$$U(t) = P(t)e^{-iH_F t}P^\dagger(0),$$

where $P(t+T) = P(t)$ is the matrix that contains the components of the Floquet states (in a given basis). In the CHRW

approximation we obtain for the matrix of Floquet states

$$P(t) = U_x^\dagger(t)R^\dagger(t)W^\dagger e^{i\frac{\omega}{2}\hat{\sigma}_z},$$

where we have taken for H_F the form

$$H_F = -\frac{\Omega_R - \omega}{2}\hat{\sigma}_z,$$

which gives the correct $\omega \rightarrow \infty$ limit.

From the columns of the $P(t)$ matrix we obtain the Floquet states

$$|u_\alpha(t)\rangle = \begin{cases} |a\rangle = \begin{pmatrix} \cos\frac{\theta}{2}\cos\frac{\phi}{2} - e^{-i\omega t}\sin\frac{\theta}{2}\sin\frac{\phi}{2} \\ i\cos\frac{\theta}{2}\sin\frac{\phi}{2} + ie^{i\omega t}\sin\frac{\theta}{2}\cos\frac{\phi}{2} \end{pmatrix} \\ |b\rangle = \begin{pmatrix} i\cos\frac{\theta}{2}\sin\frac{\phi}{2} + ie^{-i\omega t}\sin\frac{\theta}{2}\cos\frac{\phi}{2} \\ \cos\frac{\theta}{2}\cos\frac{\phi}{2} - e^{i\omega t}\sin\frac{\theta}{2}\sin\frac{\phi}{2} \end{pmatrix} \end{cases},$$

where $\theta = \arctan \tilde{A}/\tilde{\delta}$ and $\phi(t) = -\xi \frac{A}{\omega} \cos(\omega t)$ were already defined in Sec. II. The corresponding quasienergies are

$$\epsilon_{a/b} = \mp \frac{\Omega_R - \omega}{2},$$

and the so-called Floquet gap is $\Delta_F = |\epsilon_b - \epsilon_a| = |\Omega_R - \omega|$.

2. Floquet-Markov master equation and transition rates

The open system dynamics can be described by the global Hamiltonian $\mathcal{H}(t) = H_s(t) + H_b + H_{sb}$, where $H_s(t) = H_s(t+T)$ is the Hamiltonian of the qubits driven by periodic external fields with time period $T = 2\pi/\omega$. The Hamiltonian H_b corresponds to a bosonic thermal bath at temperature T_b and spectral density $J(\Omega)$. The bath is linearly coupled to the qubit system in the form $H_{sb} = \hat{O} \otimes \hat{B}$, with \hat{B} an observable of the bath and \hat{O} an observable of the system. After performing the Born and Markov approximations, a quantum master equation can be obtained [38,53,54,57–62]. In most situations (away from resonances) an additional secular approximation can be realized [38,53,54,57–62,65], leading to the quantum master equation

$$\dot{\rho} = -i[H_s(t), \rho] + \sum_{\alpha\beta} \Gamma_{\alpha\beta} \left(L_{\alpha\beta} \rho L_{\alpha\beta}^\dagger - \frac{1}{2} \{ L_{\alpha\beta}^\dagger L_{\alpha\beta}, \rho \} \right), \quad (\text{A2})$$

where $L_{\alpha\beta} = |u_\alpha(t)\rangle\langle u_\beta(t)|$ are the corresponding jump operators, and the transition rates $\Gamma_{\alpha\beta}$ can be written as

$$\Gamma_{\alpha\beta} = \sum_{q=-\infty}^{+\infty} g(\epsilon_{\alpha\beta,q}) |O_{\alpha\beta}(q)|^2, \quad (\text{A3})$$

where the q -Fourier components of the transition matrix elements are

$$O_{\alpha\beta}(q) = \frac{1}{T} \int_0^T dt \langle u_\alpha(t) | \hat{O} | u_\beta(t) \rangle e^{iq\omega t},$$

and $g(x)$ is the spectral bath correlation function, $g(x) = J(x)n_{\text{th}}(x)$, with $J(x)$ the spectral density, $n_{\text{th}}(x) = [\exp(x/k_B T) - 1]^{-1}$, and $\epsilon_{\alpha\beta,q} = \epsilon_\alpha - \epsilon_\beta + q\hbar\omega$.

In the case of a two-level system like the Hamiltonian of Eq. (A1), the relaxation rate can be obtained from Eq. (A3) as

$$\Gamma_1 = \sum_{q=-\infty}^{+\infty} g(\epsilon_{ab,q}) |O_{ab}(q)|^2 + g(\epsilon_{ba,q}) |O_{ba}(q)|^2.$$

Using that $O_{ab}(q) = [O_{ba}(-q)]^*$, we can write

$$\Gamma_1 = \sum_{q=-\infty}^{+\infty} S(\epsilon_{ab,q}) |O_{ab}(q)|^2,$$

where $S(\Omega)$ is the noise power spectrum, $S(\Omega) = g(\Omega) + g(-\Omega)$. The decoherence rate is $\Gamma_2 = \frac{\Gamma_1}{2} + \Gamma_\phi$ with the dephasing rate,

$$\Gamma_\phi = \sum_{q=-\infty}^{+\infty} g(q\omega) |O_{aa}(q) - O_{bb}(q)|^2.$$

Without loss of generality we can choose $\text{Tr}(\hat{O}) = 0$, and then $O_{aa}(q) = -O_{bb}(q)$, giving

$$\Gamma_\phi = \sum_{q \geq 0} 2S(q\omega) |O_{aa}(q)|^2.$$

For $\hat{O} = \hat{\sigma}_x$ the matrix elements are $\langle u_\alpha(t) | \hat{O} | u_\beta(t) \rangle = \langle u_\alpha(t) | \hat{\sigma}_x | \beta(t) \rangle \equiv X_{\alpha\beta}(t)$. In the CHRW approximation we obtain the expressions

$$\begin{aligned} X_{ab}(t) &= \cos^2 \frac{\theta}{2} + \sin^2 \frac{\theta}{2} \cos 2\omega t \\ &\quad - i(\sin \omega t \sin \theta \sin \phi + \sin 2\omega t \cos \phi) \\ X_{aa}(t) &= -\sin \omega t \sin \theta \cos \phi + \sin 2\omega t \sin^2 \frac{\theta}{2} \sin \phi. \end{aligned}$$

To evaluate the rates, the q Fourier components $X_{\alpha\beta}(q)$ have to be calculated. After using the expansions for $\sin \phi(t)$ and $\cos \phi(t)$,

$$\begin{aligned} \sin \phi(t) &= \sum_{l=-\infty}^{+\infty} (-1)^{l+1} J_{2l+1} e^{i(2l+1)\omega t} \\ \cos \phi(t) &= \sum_{l=-\infty}^{+\infty} (-1)^l J_{2l} e^{i2l\omega t}, \end{aligned}$$

with $J_l \equiv J_l(\xi A/\omega)$, we have

$$\begin{aligned} X_{ab}(2l+1) &= 0 \\ X_{ab}(2l) &= \frac{(-1)^{l+1}}{2} [\sin \theta (J_{2l+1} + J_{2l-1}) \\ &\quad - J_{2l-2} + J_{2l+2}] \\ &\quad + \delta_{l,0} \cos^2 \frac{\theta}{2} + \left(\frac{\delta_{l,1} + \delta_{l,-1}}{2} \right) \sin^2 \frac{\theta}{2} \\ X_{aa}(2l+1) &= \frac{i^{2l+1}}{2} \left[\sin \theta (J_{2l} + J_{2l+2}) \right. \\ &\quad \left. - \sin^2 \frac{\theta}{2} (J_{2l-1} - J_{2l+3}) \right] \\ X_{aa}(2l) &= 0. \end{aligned}$$

In the lowest approximation the relaxation rate is dominated by the $q = 0$ term, giving

$$\Gamma_1 \approx 2S(\Delta_F) |X_{ab}(0)|^2 = 2S(\Delta_F) \cos^4 \frac{\theta}{2},$$

where the noise spectrum is evaluated at the Floquet gap $\Delta_F = |\Omega_R - \omega|$. On the other hand, for the dephasing rate,

the $q = 0$ term is zero, and we have to take the next term as an approximation,

$$\begin{aligned} \Gamma_\phi &\approx 2S(\omega) |X_{aa}(1)|^2 \\ &= S(\omega) \left[(J_0 + J_2) \sin \theta + (J_1 + J_3) \sin^2 \frac{\theta}{2} \right]^2. \end{aligned}$$

APPENDIX B: OTHER APPROXIMATION METHODS TO THE DYNAMICS

The dynamics of a driven two-level system has been studied extensively over the last years. Different approximation methods have been attempted to solve the time evolution of a strongly driven qubit, given by the Hamiltonian Eq. (1) for $\epsilon(t) = A \sin(\omega t)$. In the following we review some and compare them with the CHRW approximation.

1. Double rotating frame rotating wave approximation

The dynamics can also be approximated following the approach of Refs. [43,44], where an improved (second-order) rotating wave approximation is performed to calculate the Floquet states and quasienergies, after a basis transformation to a rotating frame with a time-dependent rotation frequency and a truncation of the transformed Floquet Hamiltonian to a 2×2 matrix.

Here, we obtain the same result following a different (but equivalent) procedure, where we perform two rotation transformations of the Hamiltonian Eq. (1) and a RWA approximation at the end. We start with the x rotation $|\psi'(t)\rangle = U_x |\psi(t)\rangle$, with $U_x = e^{-i\frac{\theta}{2}\hat{\sigma}_x}$, and $\phi(t) = -\frac{A}{\omega} \cos(\omega t)$. After the rotation, the transformed Hamiltonian is $H' = U_x H U_x^\dagger + i(\partial_t U_x) U_x^\dagger$, and thus

$$H' = -\frac{\Delta}{2} (\cos \phi \hat{\sigma}_z - \sin \phi \hat{\sigma}_y). \quad (\text{B1})$$

Using the expansion of $e^{i\phi(t)}$ in terms of Bessel functions, we approximate in Eq. (B1) (neglecting the high-frequency terms)

$$\begin{aligned} \cos \phi &\approx J_0 \left(\frac{A}{\omega} \right) \\ \sin \phi &\approx -2J_1 \left(\frac{A}{\omega} \right) \cos(\omega t), \end{aligned} \quad (\text{B2})$$

and therefore

$$H' = -\frac{\Delta}{2} \left[J_0 \left(\frac{A}{\omega} \right) \hat{\sigma}_z + 2J_1 \left(\frac{A}{\omega} \right) \cos(\omega t) \hat{\sigma}_y \right].$$

The second rotation is a z rotation with the unitary operator $U_z = e^{-i\frac{\omega t}{2}\hat{\sigma}_z}$, for which we obtain

$$H'' = -\frac{\tilde{\delta}}{2} \hat{\sigma}_z + \frac{\tilde{\nu}}{2} [(1 + \cos 2\omega t) \hat{\sigma}_y - \sin 2\omega t \hat{\sigma}_x], \quad (\text{B3})$$

being $\tilde{\delta} = \Delta J_0(a) - \omega$, $\tilde{\nu} = \Delta J_1(\frac{A}{\omega})$, and $a = A/\omega$. Neglecting the fast oscillating terms with frequency 2ω (RWA approximation),

$$H'' \approx -\frac{\tilde{\delta}}{2} \hat{\sigma}_z + \frac{\tilde{\nu}}{2} \hat{\sigma}_y. \quad (\text{B4})$$

Equation (B4) can be easily diagonalized with the transformation $W = e^{-i\frac{\theta}{2}\hat{\sigma}_x}$, being $\tan \theta = \tilde{v}/\tilde{\delta}$, obtaining

$$H_d = WH''W^\dagger = -\frac{\Omega_R}{2}\hat{\sigma}_z, \quad (\text{B5})$$

with

$$\Omega_R = \sqrt{\tilde{\delta}^2 + \tilde{v}^2} = \sqrt{\left[\Delta J_0\left(\frac{A}{\omega}\right) - \omega\right]^2 + \Delta^2 J_1^2\left(\frac{A}{\omega}\right)}$$

the generalized Rabi frequency.

Taking into account the previous transformations, the evolution operator associated with Eq. (1) results in

$$U^{DR}(t) = U_x^\dagger(t)U_z^\dagger(t)W^\dagger e^{i\frac{\Omega_R t}{2}\hat{\sigma}_z} W U_z(0)U_x(0), \quad (\text{B6})$$

which after one period of the driving, $T = 2\pi/\omega$, is

$$\begin{aligned} U^{DR}(T) &= -e^{i\frac{\theta-a}{2}\hat{\sigma}_x} e^{i\frac{\pi\Omega_R}{\omega}\hat{\sigma}_z} e^{-i\frac{\theta-a}{2}\hat{\sigma}_x} \\ &= -\begin{pmatrix} \cos \alpha + i \sin \alpha \cos \tilde{\theta} & \sin \alpha \sin \tilde{\theta} \\ -\sin \alpha \sin \tilde{\theta} & \cos \alpha - i \sin \alpha \cos \tilde{\theta} \end{pmatrix}, \end{aligned} \quad (\text{B7})$$

with $\alpha = \frac{\pi\Omega_R}{\omega}$ and $\tilde{\theta} = \theta - \frac{A}{\omega}$.

We can now calculate in this approximation the transition probability between the qubit states $|0\rangle \rightarrow |1\rangle$ after a time $t = T$ as

$$P_{01}^{DR} = |\langle 1|U(T)|0\rangle|^2 = \sin^2 \tilde{\theta} \sin^2 \alpha, \quad (\text{B8})$$

which is very similar in form to the probability obtained in the CHRW approximation. (Note that here the frequency Ω_R and the angles α, θ , etc. have different expressions).

2. Magnus expansion approximation

In Ref. [10] the dynamics is approximated with a Magnus expansion [66,67]. Considering a Hamiltonian $H(t)$, the Magnus expansion for the evolution operator $U(t_f, t_i)$ from time $t = t_i$ to time $t = t_f$, with $\Delta t = t_f - t_i$, is

$$U(t_f, t_i) = \exp\{-i\tilde{H}\Delta t\}, \quad (\text{B9})$$

with

$$\tilde{H} = \tilde{H}^{(1)} + \tilde{H}^{(2)} + \tilde{H}^{(3)} + \tilde{H}^{(4)} + \dots, \quad (\text{B10})$$

where the first terms $\tilde{H}^{(n)}$ of the expansion are

$$\begin{aligned} \tilde{H}^{(1)} &= \frac{1}{\Delta t} \int_{t_i}^{t_f} dt H(t), \\ \tilde{H}^{(2)} &= \frac{1}{2i\Delta t} \int_{t_i}^{t_f} dt \int_{t_i}^t dt' [H(t), H(t')]. \end{aligned} \quad (\text{B11})$$

Since for fast gates we are interested in the evolution after one period of the drive $T = 2\pi/\omega$, the Magnus expansion can be used to estimate $U(T)$ for the Hamiltonian H given in Eq. (1). Following the approach of Ref. [10], we start by applying the transformations $|\psi'(t)\rangle = U_0|\psi(t)\rangle$, $H' = U_0 H U_0^\dagger + i(\partial_t U_0)U_0^\dagger$, with $U_0 = e^{-i\frac{\chi}{2}\hat{\sigma}_x}$, and $\chi(t) = -\frac{A}{\omega}[\cos(\omega t) - 1]$. This gives

$$H' = -\frac{\Delta}{2}(\cos \chi \hat{\sigma}_z - \sin \chi \hat{\sigma}_y). \quad (\text{B12})$$

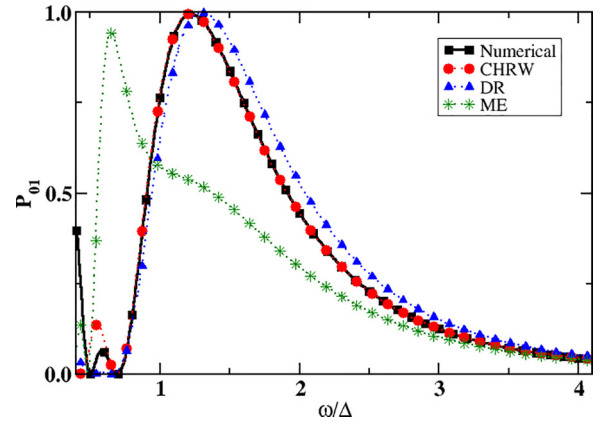


FIG. 8. Plot of the transition probability P_{01} as a function of ω/Δ for $A = 1.16\Delta$ comparing different approximation methods. Black squares: numerically exact values. Red circles: CHRW, as given by Eq. (11). Blue triangles: double rotating frame rotating wave approximation (DR), as given by Eq. (B8). Green stars: Magnus expansion approximation (ME), first order, as given by Eq. (B13).

For the evolution after one period $T = 2\pi/\omega$ we consider the lowest order in the Magnus expansion:

$$U'(T) \approx e^{-i\frac{1}{T} \int_0^T dt H'(t)}.$$

The Magnus expansion converges for $\|H(t)\|\Delta t \ll 1$, which in this case corresponds to the high-frequency limit $\Delta \ll \omega$. Thus, one obtains [10]

$$U'(T) \approx -\begin{pmatrix} \cos \alpha + i \sin \alpha \cos \theta & \sin \alpha \sin \theta \\ -\sin \alpha \sin \theta & \cos \alpha - i \sin \alpha \cos \theta \end{pmatrix},$$

with $\alpha = \pi\Omega_R^{(0)}/\omega$, $\theta = A/\omega$, and $\Omega_R^{(0)} = \Delta J_0(\frac{A}{\omega})$. Since $U_0(0) = U_0(T) = I$, the evolution operator is $U(T) = U_0(T)U(T)U_0^\dagger(0) = U'(T)$. Therefore, the transition probability P_{01} in this first-order Magnus expansion approximation is

$$\begin{aligned} P_{01}^{ME} &= |\langle 1|U(T)|0\rangle|^2 = \sin^2 \theta \sin^2 \alpha \\ &= \sin^2 \left(\frac{A}{\omega}\right) \sin^2 \frac{\pi \Delta J_0\left(\frac{A}{\omega}\right)}{\omega}. \end{aligned} \quad (\text{B13})$$

3. Comparison of the different approximations

We now compare the different approximations for the calculation of the transition probability P_{01} . In Fig. 8 we show P_{01} as a function of the frequency ω for $A = 1.16\Delta$. We plot the numerically exact values obtained with a highly accurate fourth-order Trotter-Suzuki algorithm [41]. We find that the first-order ME approximation of Eq. (B13) only agrees with the exact results for $\omega \gtrsim 3\Delta$. On the other hand, the DR approximation of Eq. (B8) agrees reasonably well with the exact dependence with frequency, with errors $\propto 10^{-2}$ in the frequencies of interest and improving accuracy for large frequencies.

The CHRW approximation is very accurate for $\omega \gtrsim \Delta$, and it is almost indistinguishable from the exact results in the scale of the plot. From Fig. 2 one can see that for this amplitude and $\omega \gtrsim \Delta$ the error is $\mathcal{E} < 10^{-5}$.

- [1] P. Krantz, M. Kjaergaard, F. Yan, T. P. Orlando, S. Gustavsson, and W. D. Oliver, *Appl. Phys. Rev.* **6**, 021318 (2019).
- [2] M. Kjaergaard, M. Schwartz, J. Braumüller, P. Krantz, J. I.-J. Wang, S. Gustavsson, and W. Oliver, *Annu. Rev. Condens. Matter Phys.* **11**, 369 (2020).
- [3] S. Kwon, A. Tomonaga, G. Lakshmi Bhai, S. J. Devitt, and J.-S. Tsai, *J. Appl. Phys.* **129**, 041102 (2021).
- [4] J. Koch, T. M. Yu, J. Gambetta, A. A. Houck, D. I. Schuster, J. Majer, A. Blais, M. H. Devoret, S. M. Girvin, and R. J. Schoelkopf, *Phys. Rev. A* **76**, 042319 (2007).
- [5] F. Yan, S. Gustavsson, A. Kamal, J. Birenbaum, A. P. Sears, D. Hover, T. J. Gudmundsen, D. Rosenberg, G. Samach, S. Weber *et al.*, *Nat. Commun.* **7**, 12964 (2016).
- [6] A. Manucharyan, J. Koch, L. I. Glazman, and M. H. Devoret, *Science* **326**, 113 (2009).
- [7] I. M. Pop, K. Geerlings, G. Catelani, R. J. Schoelkopf, L. I. Glazman, and M. H. Devoret, *Nature (London)* **508**, 369 (2014).
- [8] L. B. Nguyen, Y.-H. Lin, A. Somoroff, R. Mencia, N. Grabon, and V. E. Manucharyan, *Phys. Rev. X* **9**, 041041 (2019).
- [9] F. Bao, H. Deng, D. Ding, R. Gao, X. Gao, C. Huang, X. Jiang, H.-S. Ku, Z. Li, X. Ma, X. Ni, J. Qin, Z. Song, H. Sun, C. Tang, T. Wang, F. Wu, T. Xia, W. Yu, F. Zhang *et al.*, *Phys. Rev. Lett.* **129**, 010502 (2022).
- [10] D. K. Weiss, H. Zhang, C. Ding, Y. Ma, D. I. Schuster, and J. Koch, *PRX Quantum* **3**, 040336 (2022).
- [11] A. Somoroff, Q. Ficheux, R. A. Mencia, H. Xiong, R. Kuzmin, and V. E. Manucharyan, *Phys. Rev. Lett.* **130**, 267001 (2023).
- [12] P. J. Leek, J. M. Fink, A. Blais, R. Bianchetti, M. Göppl, J. M. Gambetta, D. I. Schuster, L. Frunzio, R. J. Schoelkopf, and A. Wallraff, *Science* **318**, 1889 (2007).
- [13] J. Bylander, S. Gustavsson, F. Yan, F. Yoshihara, K. Harrabi, G. Fitch, D. G. Cory, Y. Nakamura, J.-S. Tsai, and W. D. Oliver, *Nat. Phys.* **7**, 565 (2011).
- [14] Y.-C. Yang, S. N. Coppersmith, and M. Friesen, *Phys. Rev. A* **95**, 062321 (2017).
- [15] Y. Wang, C. Guo, G.-Q. Zhang, G. Wang, and C. Wu, *Sci. Rep.* **7**, 44251 (2017).
- [16] D. Zhu, T. Jaako, Q. He, and P. Rabl, *Phys. Rev. Appl.* **16**, 014024 (2021).
- [17] P. Shen, T. Chen, and Z.-Y. Xue, *Phys. Rev. Appl.* **16**, 044004 (2021).
- [18] Q. Ficheux, L. B. Nguyen, A. Somoroff, H. Xiong, K. N. Nesterov, M. G. Vavilov, and V. E. Manucharyan, *Phys. Rev. X* **11**, 021026 (2021).
- [19] M. Bastrakova, N. Klenov, V. Ruzhickiy, I. Soloviev, and A. Satanin, *Supercond. Sci. Technol.* **35**, 055003 (2022).
- [20] Y.-H. Chen, A. Miranowicz, X. Chen, Y. Xia, and F. Nori, *Phys. Rev. Appl.* **18**, 064059 (2022).
- [21] F. Bloch and A. Siegert, *Phys. Rev.* **57**, 522 (1940).
- [22] C. Avinadav, R. Fischer, P. London, and D. Gershoni, *Phys. Rev. B* **89**, 245311 (2014).
- [23] D. L. Campbell, Y.-P. Shim, B. Kannan, R. Winik, D. K. Kim, A. Melville, B. M. Niedzielski, J. L. Yoder, C. Tahan, S. Gustavsson, and W. D. Oliver, *Phys. Rev. X* **10**, 041051 (2020).
- [24] H. Zhang, S. Chakram, T. Roy, N. Earnest, Y. Lu, Z. Huang, D. K. Weiss, J. Koch, and D. I. Schuster, *Phys. Rev. X* **11**, 011010 (2021).
- [25] A. Petrescu, C. Le Calonnec, C. Leroux, A. Di Paolo, P. Mundada, S. Sussman, A. Vrajitoarea, A. A. Houck, and A. Blais, *Phys. Rev. Appl.* **19**, 044003 (2023).
- [26] W. D. Oliver, Y. Yu, J. C. Lee, K. K. Berggren, L. S. Levitov, and T. P. Orlando, *Science* **310**, 1653 (2005).
- [27] M. Sillanpää, T. Lehtinen, A. Paila, Y. Makhlin, and P. Hakonen, *Phys. Rev. Lett.* **96**, 187002 (2006).
- [28] A. Ferrón, D. Domínguez, and M. J. Sánchez, *Phys. Rev. Lett.* **109**, 237005 (2012).
- [29] S. N. Shevchenko, A. N. Omelyanchouk, and E. Il'ichev, *Low Temp. Phys.* **38**, 283 (2012).
- [30] O. V. Ivakhnenko, S. N. Shevchenko, and F. Nori, *Phys. Rep.* **995**, 1 (2023).
- [31] W. D. Oliver and S. O. Valenzuela, *Quant. Info. Proc.* **8**, 261 (2009).
- [32] D. M. Berns, M. S. Rudner, S. O. Valenzuela, K. K. Berggren, W. D. Oliver, L. S. Levitov, and T. P. Orlando, *Nature (London)* **455**, 51 (2008).
- [33] J. Bylander, M. S. Rudner, A. V. Shytov, S. O. Valenzuela, D. M. Berns, K. K. Berggren, L. S. Levitov, and W. D. Oliver, *Phys. Rev. B* **80**, 220506(R) (2009).
- [34] S. Gustavsson, J. Bylander, and W. D. Oliver, *Phys. Rev. Lett.* **110**, 016603 (2013).
- [35] A. L. Gramajo, D. Campbell, B. Kannan, D. K. Kim, A. Melville, B. M. Niedzielski, J. L. Yoder, M. J. Sánchez, D. Domínguez, S. Gustavsson, and W. D. Oliver, *Phys. Rev. Appl.* **14**, 014047 (2020).
- [36] J. H. Shirley, *Phys. Rev.* **138**, B979 (1965).
- [37] S.-K. Son, S. Han, and S.-I. Chu, *Phys. Rev. A* **79**, 032301 (2009).
- [38] A. Ferrón, D. Domínguez, and M. J. Sánchez, *Phys. Rev. B* **93**, 064521 (2016).
- [39] Y. Yan, Z. Lu, and H. Zheng, *Phys. Rev. A* **91**, 053834 (2015).
- [40] Z. Lü and H. Zheng, *Phys. Rev. A* **86**, 023831 (2012).
- [41] N. Hatano and M. Suzuki, Finding exponential product formulas of higher orders, in *Quantum Annealing and Other Optimization Methods*, edited by A. Das and B. K. Chakrabarti (Springer, Berlin, Heidelberg, 2005), Vol. 679, pp. 37–68.
- [42] L. H. Pedersen, N. M. Møller, and K. Mølmer, *Phys. Lett. A* **367**, 47 (2007).
- [43] C. Deng, J.-L. Orgiazzi, F. Shen, S. Ashhab, and A. Lupascu, *Phys. Rev. Lett.* **115**, 133601 (2015).
- [44] C. Deng, F. Shen, S. Ashhab, and A. Lupascu, *Phys. Rev. A* **94**, 032323 (2016).
- [45] D. C. McKay, C. J. Wood, S. Sheldon, J. M. Chow, and J. M. Gambetta, *Phys. Rev. A* **96**, 022330 (2017).
- [46] C. Huang, T. Wang, F. Wu, D. Ding, Q. Ye, L. Kong, F. Zhang, X. Ni, Z. Song, Y. Shi, H.-H. Zhao, C. Deng, and J. Chen, *Phys. Rev. Lett.* **130**, 070601 (2023).
- [47] I. N. Moskaleenko, I. S. Besedin, I. A. Simakov, and A. V. Ustinov, *Appl. Phys. Lett.* **119**, 194001 (2021).
- [48] I. N. Moskaleenko, I. A. Simakov, N. N. Abramov, A. A. Grigorev, D. O. Moskalev, A. A. Pishchimova, N. S. Smirnov, E. V. Zikiy, I. A. Rodionov, and I. S. Besedin, *npj Quantum Inf.* **8**, 130 (2022).
- [49] S. Poletto, J. M. Gambetta, S. T. Merkel, J. A. Smolin, J. M. Chow, A. D. Córcoles, G. A. Keefe, M. B. Rothwell, J. R. Rozen, D. W. Abraham, C. Rigetti, and M. Steffen, *Phys. Rev. Lett.* **109**, 240505 (2012).
- [50] M. Roth, M. Ganzhorn, N. Moll, S. Filipp, G. Salis, and S. Schmidt, *Phys. Rev. A* **96**, 062323 (2017).

- [51] K. N. Nesterov, Q. Ficheux, V. E. Manucharyan, and M. G. Vavilov, *PRX Quantum* **2**, 020345 (2021).
- [52] J. M. Chow, J. M. Gambetta, L. Tornberg, J. Koch, L. S. Bishop, A. A. Houck, B. R. Johnson, L. Frunzio, S. M. Girvin, and R. J. Schoelkopf, *Phys. Rev. Lett.* **102**, 119901(E) (2009).
- [53] S. Kohler, R. Utermann, P. Hänggi, and T. Dittrich, *Phys. Rev. E* **58**, 7219 (1998).
- [54] J. Hausinger and M. Grifoni, *Phys. Rev. A* **81**, 022117 (2010).
- [55] F. Yan, S. Gustavsson, J. Bylander, X. Jin, F. Yoshihara, D. G. Cory, Y. Nakamura, T. P. Orlando, and W. D. Oliver, *Nat. Commun.* **4**, 2337 (2013).
- [56] F. Yoshihara, Y. Nakamura, F. Yan, S. Gustavsson, J. Bylander, W. D. Oliver, and J.-S. Tsai, *Phys. Rev. B* **89**, 020503(R) (2014).
- [57] M. Grifoni and P. Hänggi, *Phys. Rep.* **304**, 229 (1998).
- [58] S. Kohler, T. Dittrich, and P. Hänggi, *Phys. Rev. E* **55**, 300 (1997).
- [59] H.-P. Breuer, W. Huber, and F. Petruccione, *Phys. Rev. E* **61**, 4883 (2000).
- [60] D. W. Hone, R. Ketzmerick, and W. Kohn, *Phys. Rev. E* **79**, 051129 (2009).
- [61] S. Gasparinetti, P. Solinas, S. Pugnetti, R. Fazio, and J. P. Pekola, *Phys. Rev. Lett.* **110**, 150403 (2013).
- [62] S. Gasparinetti, P. Solinas, A. Braggio, and M. Sassetti, *New J. Phys.* **16**, 115001 (2014).
- [63] A. Ferrón and D. Domínguez, *Phys. Rev. B* **81**, 104505 (2010).
- [64] The relaxation rate decreases with A within the range of application for the proposed gates, as seen in Figs. 6 and 7. For much larger values, $A/\omega \gg 1$, it has an oscillatory behavior.
- [65] A. L. Gramajo, D. Domínguez, and M. J. Sánchez, *Phys. Rev. A* **98**, 042337 (2018).
- [66] W. Magnus, *Commun. Pure Appl. Math.* **7**, 649 (1954).
- [67] S. Blanes, F. Casas, J. Oteo, and J. Ros, *Phys. Rep.* **470**, 151 (2009).